Journal of Alloys and Compounds 509 (2011) 6083–6089

Contents lists available at ScienceDirect

Journal of Alloys and Compounds

journal homepage: www.elsevier.com/locate/jallcom

Impedance and modulus analysis of the $(Na_{0.6}Ag_{0.4})_2PbP_2O_7$ compound

Haibado Mahamoud, B. Louati*, F. Hlel, K. Guidara

University of Sfax, Laboratory of solid state, Faculty of sciences, B. P. 1171, 3000 Sfax, Tunisia

ARTICLE INFO

Article history:
Received 5 June 2010
Received in revised form 3 March 2011
Accepted 6 March 2011
Available online 11 March 2011

Keywords:
Impedance spectroscopy
Modulus
Dielectric
Equivalent circuit

ABSTRACT

The electrical properties of the $(Na_{0.6}Ag_{0.4})_2PbP_2O_7$ compound were studied using the complex impedance spectroscopy in the temperature range (502–667 K). Grain interior, grain boundary and electrode–material interface contributions to the electrical response are identified by the analysis of complex plan diagrams. The imaginary part of the modulus at several temperatures shows a double relaxation peaks, furthermore suggesting the presence of grains and grain boundaries in the sample. An analysis of the dielectric constants ε', ε'' and loss tangent $\tan(\delta)$ with frequency shows a distribution of relaxation times. The dc conductivity of the material is thermally activated with an activation energy about 0.8 eV which is in the vicinity of the that obtained from $\tan(\delta)$ ($E = 0.7$ eV) and modulus ($E_m = 0.68$ eV) studies.

1. Introduction

Solid phase inorganic phosphates constitute a family of materials that have special attention because of their large applications whose include electric, pyroelectric, ferroelectric, magnetic, catalytic processes, state laser materials, etc. [1–7]. The phosphate compounds which contain a monovalent cation have attracted researchers due to their remarkable ionic conductivity and their potential value as solid electrolytes for rechargeable alkaline batteries [8,9]. Among them, pyrophosphates with general formula $A_2BP_2O_7$ (A: monovalent element and B: divalent element) has been widely investigated. However, mixed pyrophosphate ($A_{2-x}M_xBP_2O_7$, A, M: monovalent cation) was not sufficiently studied. For this reason, we are interested to this family of compounds in order to determine the effect of the monovalent substitution on the ionic conduction.

Recently we have reported the electrical properties of the $(Na_{0.8}Ag_{0.2})_2PbP_2O_7$ [10] and $(Na_{0.5}Ag_{0.5})_2PbP_2O_7$ [11] compounds. As a continuation, we analyze in this paper, the conduction behavior and the dielectrical properties of the polycrystalline $(Na_{0.6}Ag_{0.4})_2PbP_2O_7$ sample over the frequency range 200 Hz to 5 MHz and temperature range 502–667 K.

2. Experimental

The polycrystalline sample of $(Na_{0.6}Ag_{0.4})_2PbP_2O_7$ has been prepared using the standard solid-state reaction techniques. The starting materials were Na_2CO_3, $AgNO_3$ and $NH_4H_2PO_4$ with purity 99.99%. These materials were mixed in stoichiometric ratio and progressively heated from room temperature to 473 K at first step in order to expel NH_3, H_2O and CO_2. The calcined powder was then pressed into cylindrical pellets, heated once at 623 K for 4 h and finally at 800 K. Material formation was confirmed by X-ray diffraction (XRD) study. XRD pattern of the material was recorded at room temperature using a Phillips powder diffractometer PW 1710 in a wide range of Bragg angles ($5^\circ \leq 2\theta \leq 60^\circ$) with Co radiation ($\lambda = 1.7903$ Å). A pellet of about 8 mm diameter and 1.7 mm thickness was used in the electrical measurements. Vacuum evaporated platinum was used as electrode material. The ac conductivity measurements were performed with a Tegam 3550 impedance interfaced with a computer and a temperature controller.

3. Results and discussion

3.1. Crystalline parameters

At room temperature, all the X-ray peaks were indexed in the triclinic system with $P\bar{1}$ space group ($a = 5.5059(4)$ Å, $b = 6.9176(4)$ Å, $c = 9.5241(4)$ Å, $\alpha = 105.91(2)^\circ$, $\beta = 96.48(2)^\circ$, $\gamma = 108.64(2)^\circ$ and $V = 322.468(3)$ Å^3) (Fig. 1).

3.2. Complex electrical impedance analysis

The complex impedance spectra of the $(Na_{0.6}Ag_{0.4})_2PbP_2O_7$ compound at different temperatures are shown in Fig. 2. There are two semicircles in each impedance spectrum. The low frequency semicircle is due to the grain boundary and the higher depicts the bulk (grain) effect [12]. The impedance data were fitted to an equivalent circuit consisting of series combination of grains and grains boundary elements. The first consists of parallel combination of resistance (R_g) and capacitance (C_g) whereas the second consists of parallel combination of resistance (R_{gb}) and a constant phase

* Corresponding author.
E-mail address: bassem_louati@yahoo.fr (B. Louati).

0925-8388/$ – see front matter © 2011 Elsevier B.V. All rights reserved.
doi:10.1016/j.jallcom.2011.03.027

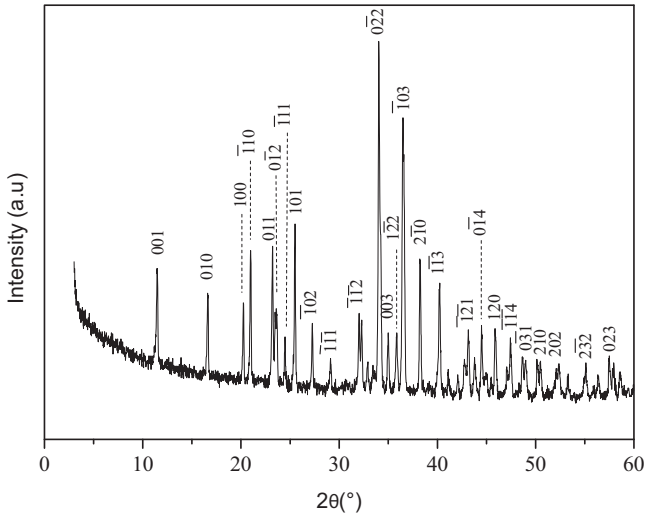

Fig. 1. X-ray diffractogram of $(Na_{0.6}Ag_{0.4})_2PbP_2O_7$ in the 2θ range 5–60°.

element CPE_{gb}. The impedance of CPE_{gb} is:

$$Z_{CPE_{gb}} = [Q_{gb}(j\omega)^{\alpha}]^{-1} \quad (1)$$

where Q_{gb} indicates the value of the capacitance of the CPE_{gb} element and α the degree of deviation with respect to the value of the pure capacitor.

An appearance of a little spike after the semicircles in the low frequency region is also noticed in the pattern at $T \geq 605$ K, which can be explained with double layer capacity, CPE_{el}, due to the electrode polarization effect. This behavior is typical of an ionically conducting polycrystalline material [13]. The appropriate equivalent circuit to the semicircles observed beyond 605 K is given in Fig. 2b.

The real and imaginary components of the whole impedance were calculated according to the following expressions:

$$Z' = \frac{R_g}{1+(\omega R_g C_g)^2} + \frac{R_{gb}^2 Q_{gb}\omega^{\alpha_{gb}}\cos(\alpha_{gb}\pi/2) + R_{gb}}{(1+R_{gb}Q_{gb}\omega^{\alpha_{gb}}\cos(\alpha_{gb}\pi/2))^2 + (R_{gb}Q_{gb}\omega^{\alpha_{gb}}\sin(\alpha_{gb}\pi/2))^2} + \frac{\cos(\alpha_{el}\pi/2)}{Q_{el}\omega^{\alpha_{el}}} \quad (2)$$

$$Z'' = R_g\frac{\omega R_g C_g}{1+(\omega R_g C_g)^2} + \frac{R_{gb}^2 Q_{gb}\omega^{\alpha_{gb}}\sin(\alpha_{gb}\pi/2)}{(1+R_{gb}Q_{gb}\omega^{\alpha_{gb}}\cos(\alpha_{gb}\pi/2))^2 + (R_{gb}Q_{gb}\omega^{\alpha_{gb}}\sin(\alpha_{gb}\pi/2))^2} + \frac{\sin(\alpha_{el}\pi/2)}{Q_{el}\omega^{\alpha_{el}}} \quad (3)$$

In these equations, the terms respects to Q_{el} are considered only for the temperature range 605–667 K. The simulated spectra according to the above equivalent circuit were represented with solid lines in Fig. 2(a) and (b). In Fig. 3(a) and (b) we show the experimental and calculated values Z' as a function of ω using the equivalent circuit. It is observed that the magnitude of Z' decreases with increasing temperature in the low frequency region and shows a negative temperature coefficient of resistance (NTCR) type behavior. At higher frequencies, the pattern shows a plateau region, i.e. frequency independent values of Z', beyond a certain frequency value depending on temperature. This particular frequency at which Z' value becomes independent of frequency is found to shift toward the higher frequency side with rise in temperature indicating the possibility of frequency relaxation process in the material. The coincidence of the Z' values at higher frequencies at all the temperatures indicates a possible release of space charge as a result of reduction in the resistive behavior of the material with rise in temperature [14].

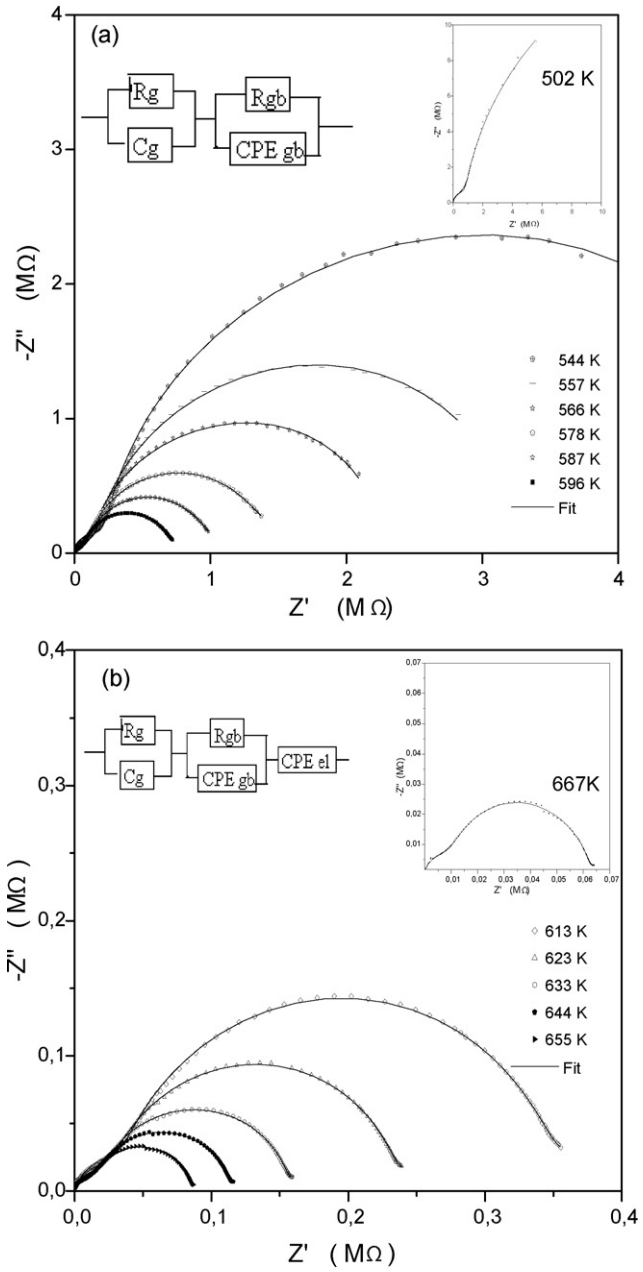

Fig. 2. Complex impedance spectra at different temperatures with electrical equivalent circuit, the solid line is a fit of the experimental data.

The angular frequency dependence of the experimental and simulated (solid line) of the imaginary part of impedance (Z'') at various temperatures is shown in Fig. 4(a) and (b). The patterns show two distinct regions which are temperature dependent. At low temperature (i.e. below 544 K), it shows a monotonic decrease in the value of Z'' without any peaks in the investigated frequency range. For the temperature at and above 544 K, the frequency dependence of Z'' is characterized by a broadening peak appearing at unique frequency that describes the type and strength of electrical relaxation phenomenon in the system [15]. The position of these peaks shifts to higher frequency with an increase of the temperature, showing thermally activated nature of the relaxation times. The broad nature of the peaks indicates multiple relaxation times in the system. The relaxation process may be due to the presence of immobile species at low temperature and defects/vacancies at higher temperature. Moreover, the magnitude of Z'' maxima decreases gradually with

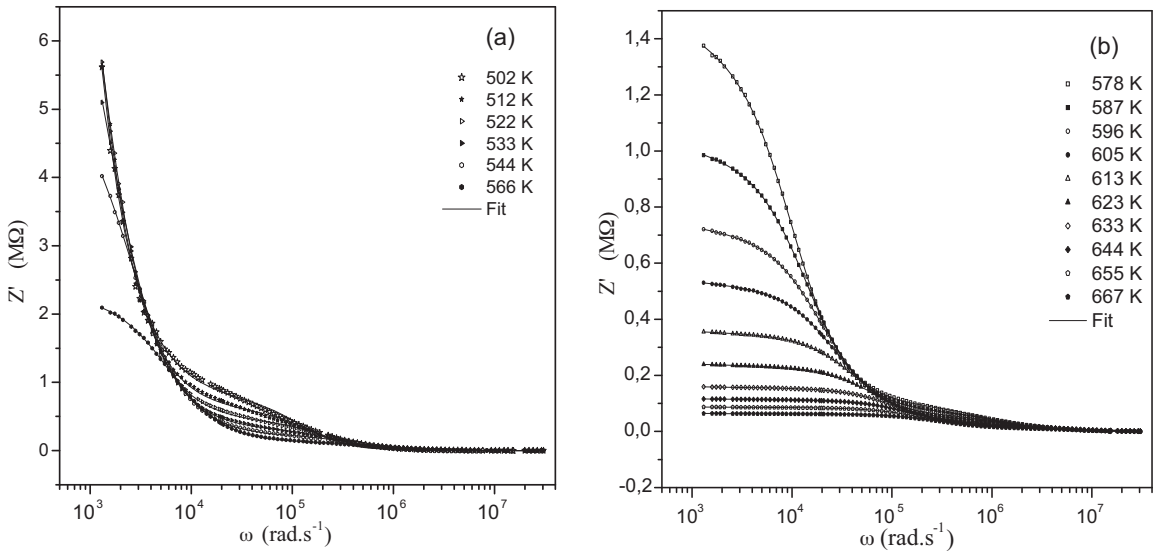

Fig. 3. Variation of the real part of the impedance as a function of angular frequency at several temperatures.

increase in both frequency and temperature and it merges finally in the high frequency region. This may possibly be an indication of the accumulation of space charge polarization effects in the material at lower frequency and at higher temperature.

Nyquist plots reported in Figs. 2–4 show a good agreement between simulated and experimental data indicating that the proposed equivalent circuit describes well the electrical properties of the sample. The extract parameters for the circuit elements are collected in Table 1. The capacitance values for the high and the low frequency semicircles are found to be in the range of 10^{-12} and $10^{-10}F$, respectively, proving that the observed semicircles represented the bulk and the grain boundary response of the system, respectively. It is evident from Table 1 and Fig. 2(b) that the grain resistance (R_g) is much lower than the grain boundary one. The resistance in the equivalent circuit is dominated by the grain-boundary resistance (R_{gb}) and hence, the semicircle of bulk is masked in a limited frequency range at higher temperature. The higher boundary resistance can be explained by the fact that the atomic arrangement near the grain boundary region is disordered, resulting in a serious increase in electron scaling.

3.3. Dielectric studies

The angular frequency dependence plots of the real and imaginary parts, ε' and ε'', of complex dielectric permittivity ε^* at several temperatures between 502 and 667 K are represented in Figs. 5 and 6. One observes that ε' approaches a limiting constant value, $\varepsilon'_\infty(\omega)$ at high frequencies, which can be interpreted as a result of a rapid polarization processes with no ionic motion contribution because the frequency is too high and the ions can only oscillate without reaching the sample–electrode interface. At lower frequencies, the ε' values increase with decreasing frequency with a rapid rise at high temperatures. In the intermediate frequency range, it shows a plateau. The rise of ε' is due to the sample–electrode interface polarization. The presence of a little spike in the complex plane impedance representation also confirms that electrode polarization is responsible for the increase of ε' at low frequency and high temperature. The intermediate-frequency plateau, which found to shift to higher frequency with increasing temperature, corresponds to the limiting low frequency dielectric constant ε'_s. The frequency dispersion in high frequency side together with the limiting

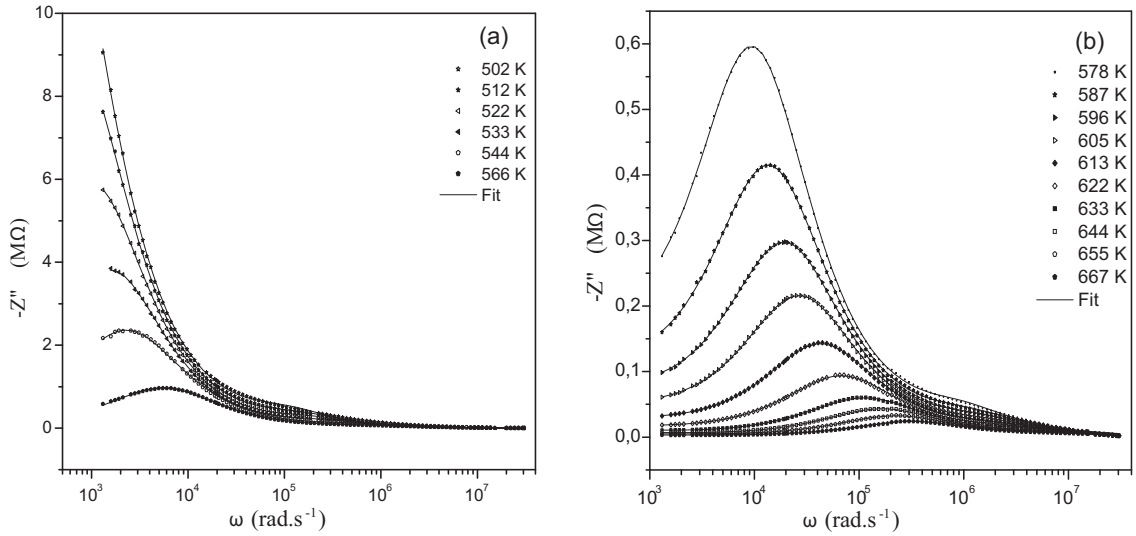

Fig. 4. Variation of the imaginary part of the impedance as a function of angular frequency at several temperatures.

Table 1
Temperature dependence of fitted circuit parameters.

T (K)	Q_{el} ($\times 10^{-6}$)	α_{el}	R_{gb} (kΩ)	Q_{gb} ($\times 10^{-10}$)	α_{gb}	R_g (kΩ)	C_g ($\times 10^{-12} F$)
502			57400	1.11	0.90	665	12.1
522			13900	1.44	0.91	384	11.8
544			5240	1.61	0.91	196	11.6
566			2190	1.82	0.90	106	11.6
574			1620	2.43	0.87	70	11.1
587			960	2.21	0.88	57	11.7
605	2.58	0.30	460	1.79	0.92	34	15.5
623	10	0.24	204	1.73	0.92	23	14.1
644	30	0.28	97	1.73	0.92	14	12.8
655	50	0.26	73	1.88	0.91	11	13.0
667	20	0.40	53	1.90	0.90	8.6	13.0

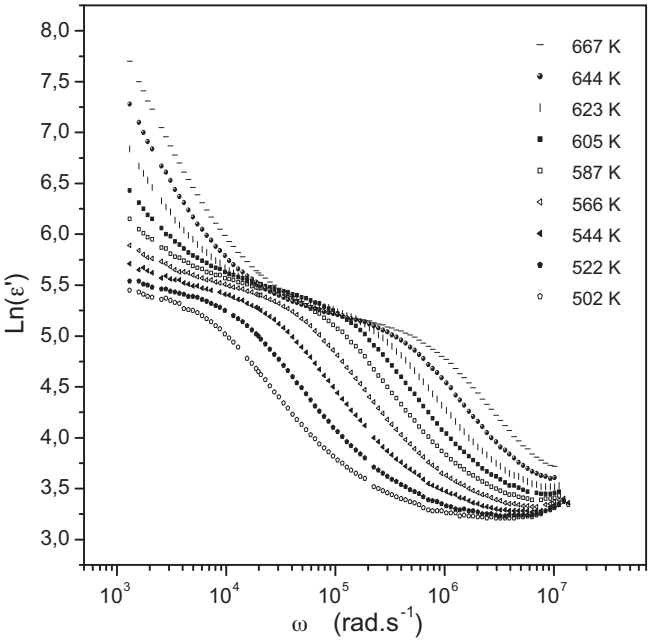

Fig. 5. Real part, ε', of the dielectric permittivity as a function of angular frequency at several temperatures.

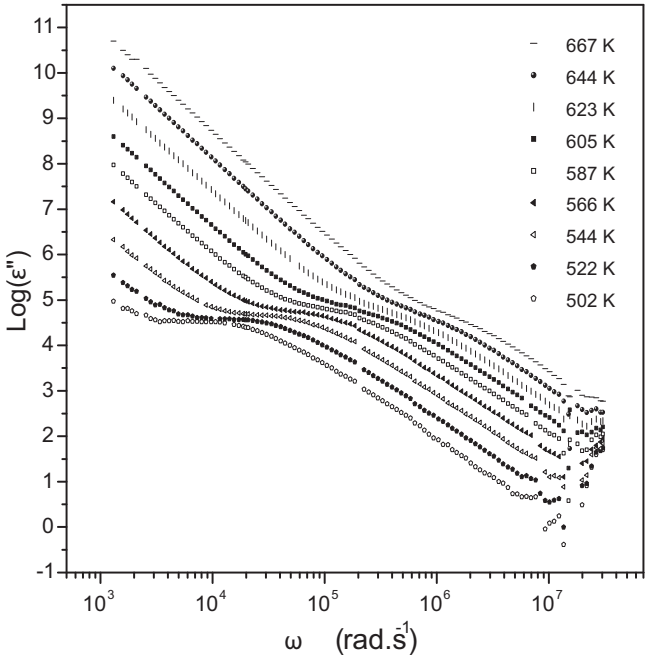

Fig. 6. Imaginary part, ε'', of the dielectric permittivity as a function of angular frequency at several temperatures.

high frequency region of ε' corresponds to the bulk polarization.

The frequency dependence of ε'' (Fig. 6) shows two straight lines with different slopes separated by frequency region. This linear behavior in both the high- and low-frequency region suggests that there are at least two processes which are contributing to the conduction of the material.

The variation of the loss tangent tan(δ) with angular frequency at selected temperatures between 502 and 667 K is given in Fig. 7. The pattern of variation is characterized by the occurrence of well defined peaks, which shifts to higher frequencies with increasing temperatures. These loss peaks and their shifts with temperature suggest a dielectric relaxation phenomenon in the material. Also, shifting of peaks toward the higher frequency sides with temperature can be attributed to a gradual decrease in resistance with increasing frequency. The temperature dependence of the peak relaxation frequency is given in Fig. 8. The slope of this straight line fit gives the values of the activation energy and is found to be 0.7 eV.

3.4. Electric modulus analysis

The electrical response of the system can be studied through complex electric modulus which is calculated using the relation: $M^*(\omega) = M' + jM''$ where $M' = \omega C_0 Z''$, and $M'' = \omega C_0 Z'$ (C_0 = geometrical capacitance).

This formalism is complementary to impedance spectroscopy and offers some advantages. It suppresses the electrode polarization and gives more importance to a circuit element having a smallest value capacitance (bulk response) when the equivalent

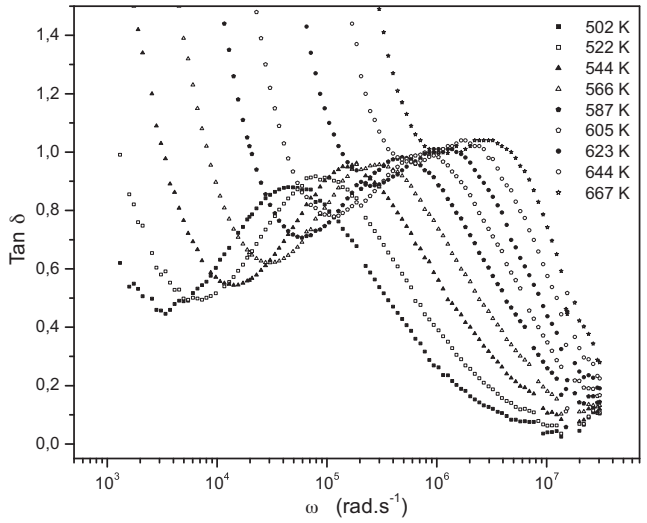

Fig. 7. Variation of tan δ with angular frequency at different temperatures.

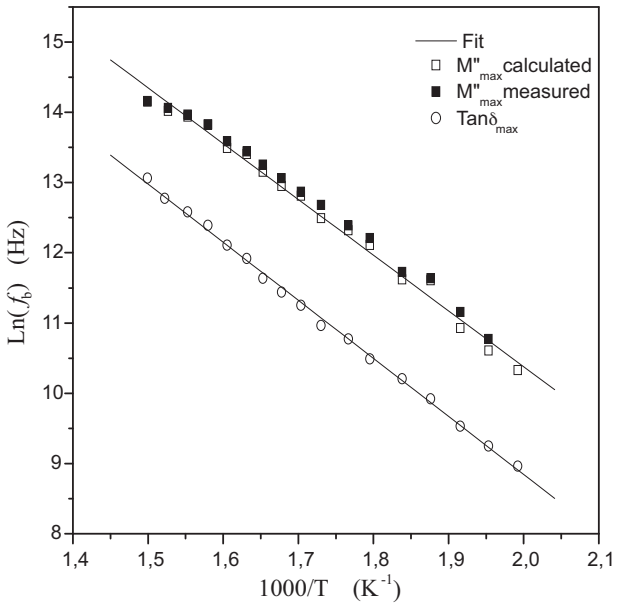

Fig. 8. Temperature dependence of the bulk relaxation frequency f_b obtained from the frequency dependent plots of tan(δ) and M'' for $(Na_{0.6}Ag_{0.4})_2PbP_2O_7$.

circuit is a several parallel-RC elements. Hence, it permits to study charge transport processes (such as mechanism of electrical transport, conductivity relaxation and ion dynamics as a function of frequency and temperature) in the grain interior via the imaginary part of modulus representation.

The variation of the imaginary part of modulus (M'') as a function of frequency at several temperatures is shown in Fig. 9. One can observe two distinct regions which are temperature dependent. In low temperature range (i.e. below 544 K), M'' spectrum shows only one relaxation peak representing the bulk grain behavior as shown in Fig. 9 inset. However, two relaxation peaks are observed in the pattern between 544 K and 667 K. Thus, the smaller peak at lower frequency is associated with grain boundary effect and the well defined one at higher frequency is correlated to the

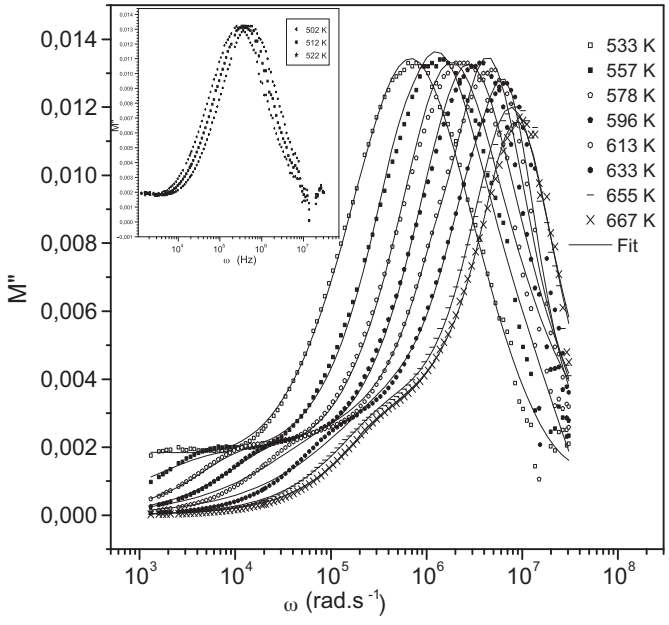

Fig. 9. Frequency dependence of the imaginary part of electric modulus at different temperatures.

bulk effects. As expected, the peak with smaller capacitance dominates the response in the modulus representation whereas in the impedance representation, the total response is totally dominated by contribution with larger resistance. The position of these relaxation peaks is found to shift to higher frequencies with the increase of the temperature showing a temperature dependent relaxation.

The maximum in the well defined peak of M'' curves corresponds to the bulk relaxation frequency f_b and defines the bulk relaxation time τ_b as $2\pi f_b \tau_b = 1$. The variation of the bulk relaxation frequency f_b with temperature, in Fig. 8, follows the Arrhenius relation [16], $f_b = f_0 \exp(-E_m/kT)$, where f_0 is the frequency at infinite temperature and E_m is the activation energy. The activation energy calculated from the slope of the plot is 0.68 eV which is in good agreement with that calculated from the loss tangent.

A conventional equation to fit the frequency dependence plot of M'' at constant temperature in a variety of materials is based on the Havriliak–Negami equation [17], i.e. the electric modulus is given by:

$$M^* = M_\infty[1 - \phi_{HN}(\omega)] = M_\infty \left[1 - \frac{1}{[1 + (i\omega\tau)^\alpha]^\gamma}\right] \quad (4)$$

where ϕ_{HN} is the Havriliak–Negami (HN) function and both HN parameters α and γ define the Kohlrausch parameter β as $\beta = (\alpha\gamma)^{1/1.23}$. In order to simulate the two relaxation peaks we have modified the above expression as:

$$M^* = M_\infty \left[1 - \frac{1}{[1 + (i\omega\tau_b)^{\alpha_b}]^{\gamma_b}}\right] + M_s \left[1 - \frac{1}{[1 + (i\omega\tau_{gb})^{\alpha_{gb}}]^{\gamma_{gb}}}\right] \quad (5)$$

where $M_\infty = 1/\epsilon_\infty$, $M_s = 1/\epsilon_s$, ϵ_∞ and ϵ_s being the high and low frequency asymptotic value of the real part of the dielectric permittivity respectively. The parameter α_b and γ_b are the shape of the high frequency peak corresponding to the bulks and α_{gb} and γ_{gb} the corresponding quantities for low frequency peak. A fairly good fit was achieved using this equation (Fig. 9). Fig. 8 reveals that experimental and fitted values (solid line) of the bulk relaxation frequency are very close.

The high frequency peak in the M'' curves is found to be asymmetric, implying a non-exponential behavior of the bulk conductivity relaxation. This type of behavior suggests the possibility that the ion migration takes place via hopping accompanied by a consequential time-dependent mobility of other charge carriers of the same type in their vicinity [18,19]. The non-exponential conductivity relaxation is well described by a Kohlrausch–Williams–Watts (KWW) function [20]:

$$\phi(t) = \exp\left[\left(\frac{-t}{\tau}\right)^\beta\right] \quad (0 < \beta < 1) \quad (6)$$

where $\phi(t)$ represents the distribution of relaxation time in ion conducting materials and τ is the conductivity relaxation time. The value of β determined from the full width half maximum (FWHM) of high frequency peak ($\beta = 1.14/\text{FWHM}$) and β obtained by fitting the M'' curve to Eq. (5) are very close. Its values are found to be temperature dependent and to be in the range of 0.65–0.99. It is clear from Table 2 that the value of β approaches 1 at high temperature, showing a tendency to an ideal behavior of the sample, whereas the temperature is reduced a departure from the ideal Debye type was noticed. In general, there are several possible sources, which cause deviations from the ideal behavior. One of the sources of non ideal behavior arises from some kind of interaction among the different charges in the system and β parameter represents most often the degree of interaction between charge carriers. The value of β becomes smaller as the cooperation between charge carriers is more extended. Otherwise, for very small charge carrier concentration, there is a poor interac-

Table 2
Temperature dependence of τ_b and β.

	T (K)									
	502	522	544	566	578	587	605	623	644	667
τ_b ($\times 10^{-6}$ s)	5.19	2.86	1.43	0.71	0.60	0.43	0.31	0.22	0.14	0.11
β	0.65	0.66	0.68	0.74	0.75	0.79	0.84	0.84	0.89	0.98

Table 3
Electrical parameters of the ceramic series $(Na_{1-x}Ag_x)_2PbP_2O_7$.

Ceramic	$x = 0$ [21]	$x = 0.2$ [10]	$x = 0.4$	$x = 0.5$ [11]	$x = 1$ [22]
E_σ (eV)	0.90	0.71	0.8	0.96	0.78
E_m (eV)	–		0.7	1.07	0.75
B (Ω^{-1} cm^{-1} K)	2×10^5	7.6×10^3	4.3×10^4	4×10^4	2×10^5

tion between ions whereas when the mobile ion concentration increases, the coupling between charge carriers is more extended. Therefore, the greater value of the β at high temperature may be due to poor interaction between the mobile ions in this temperature region. The fact that at higher temperature, the well-defined peak maximum deceases with increasing temperature (see in Fig. 9) suggests that the numbers of charge carriers are decreased at high temperature.

3.5. Electrical conductivity study

The ac conductivity was calculated from dielectric measurements using the relation $\sigma_{ac} = \omega\varepsilon_0\varepsilon' \tan\delta$ (ε_0, dielectric in free space, ε', relative dielectric constant). The conductivity of the grain is obtained from (R_g) by means of the relation:

$$\sigma = \frac{e}{R_g s}$$

where e/s represents the sample geometrical ratio. The temperature dependence of the conductivity is represented in Fig. 10 in the form of Ln(σT) versus 1000/T. An Arrhenius type behavior, $\sigma T = B\exp(-E_a/kT)$, is shown.

Both σ_{dc} and σ_{gb} increase with increasing temperature, indicating that the electrical conduction in the material is a thermally activated process. For whole studied temperature range, the bulk conductivity is higher than the grain boundary one. The value of activation energy estimated from Arrhenius plot of σ_{dc} and σ_{gb} respect to $10^3/T$ is 0.8 eV and 1.2 eV, respectively. The E_a activation energy (due to the bulk contribution) is in the vicinity of E_m and the value calculated from the loss tan(δ). The conduction mechanism in this material may be due to the hopping of charge carriers.

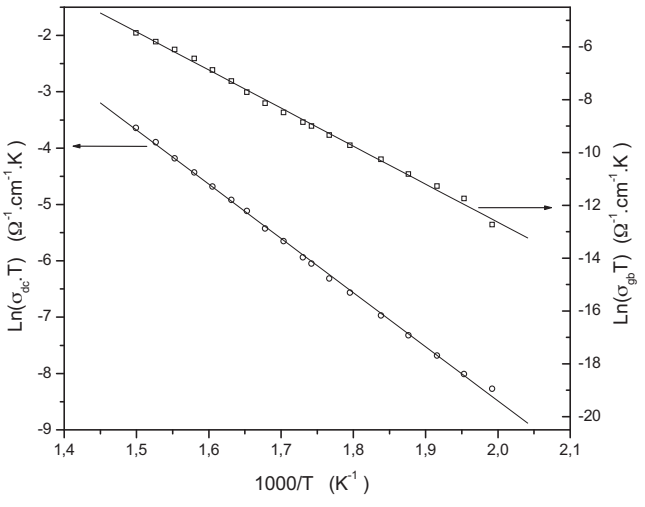

Fig. 10. Arrhenius plot of dc conductivity σ_{dc} and σ_{gb} vs 1000/T.

The electrical properties of this material can be compared with the different members of the $(Na_{1-x}Ag_x)_2PbP_2O_7$ series (Table 3). We notice an increase in the activation energy and the pre-exponential factor B with x ($0.2 \le x \le 0.5$). We noted a large difference with the parental compounds ($x = 0$ and 1), this discordance is may be due to the following points:

(i) The parental compounds and $(Na_{1-x}Ag_x)_2PbP_2O_7$ ($0.2 \le x \le 0.5$) series were prepared with different experimental procedures (difference in annealing cycles).
(ii) The specimens relative to $x = 0$ and 1 are single crystal, for ($0.2 \le x \le 0.5$) they are polycrystalline powders.
(iii) The difference between the used impedance spectrometers.

The transport properties in this material appear to be due to monovalents cations hopping mechanism along pseudo-planes parallel to (0 0 1) between-S1–S2–S2–S1-conduction paths [21,22].

4. Conclusions

The $(Na_{0.6}Ag_{0.4})_2PbP_2O_7$ synthesized by solid-state reaction technique is investigated in the temperature range 502–667 K. The X-ray diffraction analysis shows that the compound is triclinic with $P\bar{1}$ space group. Nyquists plots show: (i) both grain interior and grain boundary effect up to 605 K characterized by the appearance of two semicircular arcs in the pattern, (ii) negative temperature coefficient of resistance (NTCR)-type behavior and (iii) temperature-dependent relaxation phenomena. The presence of two relaxation peaks above 544 K in the modulus loss spectra confirmed the grain and grain boundary contribution to the electrical response in the material. The activation energy from impedance loss and modulus spectra was found to be 0.8 eV and 0.7 eV, respectively. Real and imaginary part of the dielectric permittivity shows dispersion at lower frequencies with a tendency of leveling off at intermediate frequencies, which indicates the polydispersive relaxation process in the material. The rise in both ε' and ε'' observed at low frequency and high temperature is mainly due to the electrode polarization.

References

[1] B. Aurivillius, C.I. Lindblom, P. Stenson, Acta Chem. Scand. 18 (6) (1964) 1555–1557.
[2] M. Nagpure, K.N. Shinde, V. Kumar, O.M. Ntwaeaborwa, S.J. Dhoble, H.C. Swart, J. Alloys Compd. 492 (2010) 384–388.
[3] K.V.R. Prasad, K.B.R. Varma, Ferroelectrics 158 (1994) 205–210.
[4] J.G. Chen, L. Ang, C. Wang, Y Wei, J. Alloys Compd. 478 (2009) 604–607.
[5] S. Tomohiro, H. Mikio, K. Kohei, Mater. Res. Bull. 35 (2000) 225–232.
[6] S. Tomohiro, H. Mikio, K. Kohei, O. Takayo, S. Wada, M. Hiroshi, J. Cryst. Growth 24 (2002) 159–164.

[7] T. Kanazawa, Inorganic Phosphate Materials. Materials Science Monographs, vol. 52, Elsevier, Amsterdam, 1989.
[8] A. Daidouh, M.L. Veiga, C.P. Marín, M. Martinez-Ripoll, Acta Crystallogr. C 53 (1997) 167–169.
[9] S.R.S. Prabaharan, M.S. Michael, S. Radhakrishna, C. Julien, J. Mater. Chem. 7 (1997) 1791–1796.
[10] B. Louati, F. Hlel, K. Guidara, J. Alloys Compd. 486 (2009) 299–303.
[11] M. Megdiche, H. Mahamoud, B. Louati, F. Hlel, K. Guidara, Ionics 16 (2010) 655–660.
[12] J.R. MacDonald, Impedance Spectroscopy: Emphasizing Solid Materials and Systems, John Wiley & Sons, New York, 1987, pp. 215–238.
[13] S. Brahma, R.N.P. Choudhary, A.K. Thakur, Phys. B: Phys. Cond. Matter 355 (2005) 188–201.
[14] M. Ram, Phys. B: Phys. Cond. Matter 405 (2010) 602–605.
[15] S. Chatterjee, P.K. Mahapatra, R.N.P. Choudhary, A.K. Thakur, Phys. Status Solidi (a) 201 (2004) 588–595.
[16] M.D. Migahed, N.A. Bakr, M.I. Abdel-Hamid, O. EL-Hannafy, M. El-Nimr, J. Appl. Polym. Sci. 59 (1996) 655–662.
[17] A. Oueslati, F. Hlel, K. Guidara, M. Gargouri, J. Alloys Compd. 492 (2010) 508–514.
[18] S. Saha, T.P. Sinha, Phys. Rev. B65 (2002) 134103–134107.
[19] K.P. Padmasree, D.K. Kanchan, A.R. Kkulkarni, Solid State Ionics 177 (2006) 475–482.
[20] B. Louati, K. Guidara, M. Gargouri, J. Alloys Compd. 472 (2009) 347–351.
[21] N. Dridi, A. Boukhari, J.M. Réau, E. Arbib, E.M. Holt, Solid State Ionics 127 (2000) 141–149.
[22] N. Dridi, A. Boukhari, J.M. Réau, E. Arbib, E.M. Holt, Mater. Lett. 47 (2001) 212–218.